Effect of mitochondrial circulation on mitochondrial age density distribution

Ivan A. Kuznetsov[(a), (b)] and Andrey V. Kuznetsov[(c)]

[(a)] Perelman School of Medicine, University of Pennsylvania, Philadelphia, PA 19104, USA

[(b)] Department of Bioengineering, University of Pennsylvania, Philadelphia, PA 19104, USA

[(c)] Department of Mechanical and Aerospace Engineering, North Carolina State University, Raleigh, NC 27695-7910, USA; e-mail: avkuznet@ncsu.edu

Abstract

Recent publications report that although the mitochondria population in an axon can be quickly replaced by a combination of retrograde and anterograde axonal transport (often within less than 24 h), the axon contains much older mitochondria. This suggests that not all mitochondria that reach the soma are degraded and that some are recirculating in the axon. To explain this, we developed a model that simulates mitochondria distribution when a portion of mitochondria that return to the soma are redirected back to the axon rather than being destroyed in somatic lysosomes.

Utilizing the developed model, we studied how the percentage of returning mitochondria affects the mean age and age density distributions of mitochondria at different distances from the soma. We also investigated whether turning off the mitochondria anchoring switch can reduce the mean age of mitochondria. For this purpose, we studied the effect of reducing the value of a parameter that characterizes the probability of mitochondria transition to the stationary (anchored) state. The reduction in mitochondria mean age observed when the anchoring probability is reduced suggests that some injured neurons may be saved if the percentage of stationary mitochondria is decreased. The replacement of possibly damaged stationary mitochondria with newly synthesized ones may restore the energy supply in an injured axon. We also performed a sensitivity study of the mean age of stationary mitochondria to the parameter that determines what portion of mitochondria re-enter the axon and the parameter that determines the probability of mitochondria transition to the stationary state.

Keywords: neurons; axonal transport; mean age; age density distribution; mathematical modeling

1. Introduction

The primary purpose of mitochondria in the cells is to generate easily accessible chemical energy in the form of ATP. In addition, mitochondria serve various other functions, such as calcium buffering. They are also known for their involvement in apoptosis (Fan et al. 2001; Picard and McEwen 2018).

Since mitochondrial proteins have a limited half-life, these proteins (or the entire mitochondrion) need to be periodically replaced (Misgeld and Schwarz 2017). For this reason, mitochondria are continuously transported in axons (Mogre et al. 2020). The representative length of mitochondria is between 0.5 and 10 μm (Trushina 2016); thus, mitochondria are too large to exhibit any significant diffusivity. Mitochondria transport is accomplished by molecular motors, kinesin-1 (and possibly kinesin-3) in the anterograde direction and by cytoplasmic dynein in the retrograde direction (Melkov and Abdu 2018; Kruppa and Buss 2021). Mitochondria move with an average velocity of 0.4-0.8 μm/s (Narayanareddy et al. 2014). To supply energy to energy demand sites in the axon, mitochondria can dock near these demand sites (Hollenbeck and Saxton 2005; Lees et al. 2020; Lewis et al. 2016).

Not all mitochondria that leave the axon moving retrogradely are degraded in the soma, a portion return to the axon. This is supported by the observation that after mitochondria leave the axon terminal, some of them persist in the axon for days (Mandal et al. 2021).

A high level of energy is required for neurons to survive an injury. Since the distance to which ATP can be transported by diffusion is limited, replacing damaged mitochondria with new ones is critical for neuron survival (Huang et al. 2021). Axonal regeneration after injury or ischemic stress (Ten and Galkin 2019) can be promoted by turning off mitochondria anchoring. This leads to faster replacement of damaged mitochondria with healthy mitochondria (Cheng et al. 2022). Our model simulates the reduction of mitochondria anchoring by decreasing a value of the parameter that characterizes the probability of mitochondria anchoring, p_s .

The return of mitochondria to the axon must be associated with changing the type of molecular motors that move the mitochondria. Since mitochondria are driven toward the soma by dynein motors, to turn around and re-enter the axon they must switch dynein motors to kinesin motors.

Karamched and Bressloff (2017) used mean-field equations to study the delivery of motor-cargo complexes to branched axons. A quantity called mitochondrial health was introduced by Patel et

al. (2013) and treated as a proxy for mitochondrial membrane potential. Models that treat mitochondrial health as a decaying component were developed by Agrawal and Koslover (2021).

In this paper, we follow a different approach. We use a different, compartment-based model, which simulates mitochondria transport between various demand sites. Each demand site is represented by three compartments containing populations of anterograde, stationary, and retrograde mitochondria. We developed this model in our previous publications and utilized it for determining the mean age of mitochondria along the axon length (Kuznetsov and Kuznetsov 2022a) and for computing the mean age and age density distributions of mitochondria in a branching axon (Kuznetsov and Kuznetsov 2022b).

The main question that we ask in this paper is how the mean age and age density distributions of mitochondria in the compartments located at different distances from the soma are affected by some of the mitochondria that exit the axon changing the motors that propel them to kinesin and returning to the circulation. This would explain the presence of older mitochondria in the axon, reported, for example, by Mandal et al. (2021). Intuitively, this should increase the mean age of mitochondria in the axon as a result of the described process in which older mitochondria re-enter the axon. Another question we attempt to answer in this paper is whether making mitochondria less likely to stop would contribute to a faster renewal of mitochondria (which in our model will appear as a reduction of the mean age of mitochondria). This would improve chances for neuron recovery after ischemic stress or injury (Cheng et al. 2022).

2. Materials and models

2.1. Problem setup

Mitochondria usually dock near energy demand sites in the axon (Safiulina and Kaasik 2013). We simulated the axon as consisting of N demand sites (Fig. 1). Mitochondria in the axon can be divided into stationary, anterograde, and retrograde, with transitions possible between these three pools (Hollenbeck and Saxton 2005). We therefore represented each demand site as that consisting of three compartments which contain stationary, anterograde, and retrograde mitochondria. The total number of compartments in our multi-compartment model (Anderson 1983; Jacquez 1985; Jacquez and Simon 1993) is thus $3N$, see Fig. 2 (we used N=10).

The main reason we resort to using a multi-compartment model is our desire to use the methodology for computing the age density distribution for cargos in the compartments

developed by Metzler et al. (2018) and Metzler and Sierra (2018). We used a similar approach to simulate transport of dense core vesicles in *Drosophila* motoneurons (Kuznetsov and Kuznetsov 2019; Kuznetsov and Kuznetsov 2020). The demand sites in the axon terminal were numbered from the most proximal (site 1) to the most distal (site *N*) (Fig. 1).

To characterize mitochondria concentration in the axon, we used the total length of mitochondria in a particular kinetic state (Fig. 2) per unit axon length, measured in (μm of mitochondria)/μm. The dependent variables utilized in the model are given in Table S1.

2.2. Governing equations and the model for the mean age and age density distributions of mitochondria in the demand sites

The total length of mitochondria is a conserved quantity. The equations stating the conservation of the total length of mitochondria in 3*N* compartments (Fig. 2) are stated using the methodology developed by Anderson (1983). In a vector form, these equations are

$$\frac{d}{dt}\mathbf{C}^*(t) = \mathrm{B}\left(\mathbf{C}^*(t), t\right)\mathbf{C}^*(t) + \mathbf{u}(t), \tag{1}$$

where t is the time and $\mathbf{C}^*$ is the state vector, following the terminology used in Metzler et al. (2018). $\mathbf{C}^*$ is a column vector; its components are defined as follows:

$$C_1^* = l_1 L_1, \ldots, C_N^* = l_N L_N, C_{N+1}^* = l_1^a L_1, \ldots, C_{2N-1}^* = l_{N-1}^a L_{N-1}, C_{2N}^* = l_N^m L_N, C_{2N+1}^* = l_1^r L_1, \ldots, C_{3N}^* = l_N^r L_N. \tag{2}$$

In Eq. (2)

$$\hat{l}_1 = l_1, \ldots, \hat{l}_N = l_N, \hat{l}_{N+1} = l_1^a, \ldots, \hat{l}_{2N-1} = l_{N-1}^a, \hat{l}_{2N} = l_N^m, \hat{l}_{2N+1} = l_1^r, \hat{l}_{3N} = l_N^r, \tag{3}$$

where l_i is the total length of mitochondria per unit length of the axon in stationary, anterograde, or retrograde states in the compartment by the *i*th demand site (Table S1).

Model parameters are summarized in Table S2. In Eq. (2) L_i (i=1,…,N) is the length of an axonal compartment around the *i*th demand site. Since the axonal length L_{ax} was split into N compartments of equal length, $L_i = L_{ax} / N$.

The first N components of the state vector represent the total length of mitochondria in stationary states, the next N components (N+1,…,2N) represent the total length of mitochondria in anterograde states, and the last N components (2N+1,…,3N) represent the total length of

mitochondria in retrograde states. The definition of vector $\mathbf{u}(t)$ is given below in Eqs. (45) and (46).

Matrix B(3*N*,3*N*) is composed following Anderson (1983). It accounts for the internal mitochondria fluxes between the compartments, the external mitochondria flux entering the axon from the soma, and the mitochondria flux leaving the axon, part of which returns to the soma for degradation and part re-enters the axon (Fig. 2). The analysis of mitochondria fluxes to and from the stationary, anterograde, and retrograde compartments surrounding the most proximal demand site gives equations for the following elements of matrix B:

$$b_{1,1} = -L_1 k_w l_1^s / \left(L_1 l_1^s\right), \tag{4}$$

where k_w is the kinetic constant characterizing the rate of mitochondria re-release from the stationary state into the mobile states.

$$b_{N+1,N+1} = -\left(p_s j_{soma\to 1} + j_{1\to 2}\right) / \left(L_1 l_1^a\right), \tag{5}$$

where *j* denotes the flux of mitochondria length between the compartments and p_s is the probability of mitochondria transitioning from a moving to the stationary state.

$$b_{N+1,2N+1} = \alpha j_{1\to soma} / \left(L_1 l_1^r\right), \tag{6}$$

where $j_{soma\to 1}$ is the total flux of anterograde mitochondria entering the most proximal demand site, which consists of mitochondria newly synthesized in the soma and mitochondria returning from their journey in the axon. Our model assumes that a portion of mitochondrial flux exiting the axon, $\alpha j_{1\to soma}$, returns to the axon while the other portion of the flux, $(1-\alpha) j_{1\to soma}$, is degraded in somatic lysosomes.

$$b_{2N+1,2N+1} = -\left(p_s j_{2\to 1} + (1-\alpha) j_{1\to soma}\right) / \left(L_1 l_1^r\right), \tag{7}$$

$$b_{N+1,1} = \varepsilon L_1 k_w l_1^s / \left(L_1 l_1^s\right), \tag{8}$$

where ε is the portion of mitochondria that re-enter the anterograde component and $(1-\varepsilon)$ is the portion of mitochondria that re-enter the retrograde component (Fig. 2, Table S2).

$$b_{1,N+1} = p_s j_{soma\to 1} / \left(L_1 l_1^a\right), \tag{9}$$

$$b_{2N+1,1} = (1-\varepsilon) L_1 k_w l_1^s / (L_1 l_1^s), \tag{10}$$

$$b_{1,2N+1} = p_s j_{2\to 1} / (L_1 l_1^r), \tag{11}$$

$$b_{N+2,N+1} = j_{1\to 2} / (L_1 l_1^a), \tag{12}$$

$$b_{2N+1,2N+2} = j_{2\to 1} / (L_2 l_2^r). \tag{13}$$

By analyzing mitochondria fluxes to and from the compartments surrounding demand site *i* (*i*=2,…,*N*-1), equations for the following elements of matrix B are obtained:

$$b_{i,i} = -L_i k_w l_i^s / (L_i l_i^s), \tag{14}$$

$$b_{N+i,N+i} = -(p_s j_{i-1\to i} + j_{i\to i+1}) / (L_i l_i^a), \tag{15}$$

$$b_{2N+i,2N+i} = -(p_s j_{i+1\to i} + j_{i\to i-1}) / (L_i l_i^r), \tag{16}$$

$$b_{N+i,i} = \varepsilon L_i k_w l_i^s / (L_i l_i^s), \tag{17}$$

$$b_{i,N+i} = p_s j_{i-1\to i} / (L_i l_i^a), \tag{18}$$

$$b_{2N+i,i} = (1-\varepsilon) L_i k_w l_i^s / (L_i l_i^s), \tag{19}$$

$$b_{i,2N+i} = p_s j_{i+1\to i} / (L_i l_i^r), \tag{20}$$

$$b_{N+i,N+i-1} = j_{i-1\to i} / (L_{i-1} l_{i-1}^a), \tag{21}$$

$$b_{N+i+1,N+i} = j_{i\to i+1} / (L_i l_i^a), \tag{22}$$

$$b_{2N+i-1,2N+i} = j_{i\to i-1} / (L_i l_i^r), \tag{23}$$

$$b_{2N+i,2N+i+1} = j_{i+1\to i} / (L_{i+1} l_{i+1}^r). \tag{24}$$

The analysis of mitochondria fluxes to and from the compartments surrounding the most distal demand site gives equations for the following elements of matrix B:

$$b_{N,N} = -L_N k_w l_N^s / (L_N l_N^s), \tag{25}$$

$$b_{2N,2N} = -(p_s j_{N-1\to N} + j_{N\to 3N}) / (L_N l_N^a), \tag{26}$$

$$b_{3N,3N} = -\left(p_s j_{N\to 3N} + j_{N\to N-1}\right) / \left(L_N l_N^r\right), \tag{27}$$

$$b_{2N,N} = \varepsilon L_N k_w l_N^s / \left(L_N l_N^s\right), \tag{28}$$

$$b_{N,2N} = p_s j_{N-1\to N} / \left(L_N l_N^a\right), \tag{29}$$

$$b_{2N,2N-1} = j_{N-1\to N} / \left(L_{N-1} l_{N-1}^a\right), \tag{30}$$

$$b_{3N,2N} = j_{N\to 3N} / \left(L_N l_N^a\right), \tag{31}$$

$$b_{3N,N} = \left(1-\varepsilon\right) L_N k_w l_N^s / \left(L_N l_N^s\right), \tag{32}$$

$$b_{N,3N} = p_s j_{N\to 3N} / \left(L_N l_N^r\right), \tag{33}$$

$$b_{3N-1,3N} = j_{N\to N-1} / \left(L_N l_N^r\right). \tag{34}$$

Other elements of matrix B, except for those given by Eqs. (4)-(34), are equal to zero.

Eqs. (4)-(34) were supplemented by the following equations that simulate fluxes of mobile mitochondria between the demand sites. Equations for anterograde fluxes (Fig. 2) are given by the following equations:

$$j_{1\to 2} = v_a l_1^a, \tag{35}$$

…

$$j_{i-1\to i} = v_a l_{i-1}^a, \tag{36}$$

$$j_{i\to i+1} = v_a l_i^a, \tag{37}$$

…

$$j_{N-1\to N} = v_a l_{N-1}^a, \tag{38}$$

$$j_{N\to 3N} = v_a l_N^a. \tag{39}$$

Equations for retrograde fluxes (Fig. 2) are given by the following equations:

$$j_{N\to N-1} = v_r l_N^r, \tag{40}$$

…

$$j_{i+1\to i} = v_r l_{i+1}^r, \tag{41}$$

$$j_{i\to i-1} = v_r l_i^r \,, \tag{42}$$

…

$$j_{2\to 1} = v_r l_2^r \,, \tag{43}$$

$$j_{1\to soma} = v_r l_1^r \,. \tag{44}$$

The N+1th element of column vector **u** is given by the following equation:

$$u_{N+1} = j_{soma\to 1} - \alpha\, j_{1\to soma} \,. \tag{45}$$

In Eq. (45) $j_{soma\to 1}$ is the total flux of anterograde mitochondria entering the most proximal demand site. It consists of mitochondria newly synthesized in the soma and mitochondria that just left the axon and re-enter the axon anterogradely. Eq. (45) means that the flux of newly synthesized mitochondria entering the axon from the soma, u_{N+1}, is adjusted in our model depending on the flux of mitochondria that re-entered the axon after leaving it retrogradely, $\alpha\, j_{1\to soma}$. This is done to keep the total flux of mitochondria entering the axon (newly synthesized plus returning) constant and independent of α.

The only flux entering the compartmental system displayed in Fig. 2 is the flux of newly synthesized mitochondria entering the N+1th compartment. Therefore, all other elements of vector **u** are equal to zero:

$$u_i = 0 \quad (i=1,\ldots,N,N+2,\ldots,3N-1). \tag{46}$$

We used the formulas reported in Metzler and Sierra (2018) to obtain results for the steady-state situation (when the left-hand side of Eq. (1) is equal to zero). The solution of Eq. (1) for a steady-state situation is given by the following equation:

$$\mathbf{C}_{ss}^{*} = -\mathrm{B}_{ss}^{-1}\mathbf{u}_{ss} \,. \tag{47}$$

In Eq. (47), the superscript -1 on a matrix denotes the inverse of the matrix and the subscript *ss* denotes steady-state.

The mean ages and age density distributions of mitochondria in various demand sites were computed using the method described by Metzler et al. (2018) and Metzler and Sierra (2018). The mean ages of mitochondria in various compartments displayed in Fig. 2 at steady-state are found from the following equation:

$$\overline{\mathbf{c}}_{ss} = -\left(\hat{\mathbf{C}}^{*}_{ss}\right)^{-1} \mathrm{B}_{ss}^{-1}\mathbf{C}^{*}_{ss} \,. \tag{48}$$

In Eq. (48)

$$\hat{\mathbf{C}}^{*}_{ss} = \mathrm{diag}\left(C^{*}_{1,ss}, C^{*}_{2,ss}, ..., C^{*}_{3N,ss}\right) \tag{49}$$

is the diagonal matrix with the components of the state vector, defined in Eq. (2), on the main diagonal. These components ($C^{*}_{1,ss}$, $C^{*}_{2,ss}$, etc.) are calculated at steady-state. The left-hand side of Eq. (48) is a column vector composed of the mean ages of mitochondria in various compartments:

$$\overline{\mathbf{c}}_{ss} = \left(\overline{c}_{1,ss}, ..., \overline{c}_{3N,ss}\right)^{T} , \tag{50}$$

where superscript T denotes the transposed matrix.

The age densities of mitochondria in various compartments are given by the elements of the following vector:

$$\mathbf{p}_{ss}\left(c\right) = \left(\hat{\mathbf{C}}^{*}_{ss}\right)^{-1} \mathrm{e}^{c\mathrm{B}_{ss}} \mathbf{u}_{ss} \,, \tag{51}$$

where e is the matrix exponential.

Eqs. (47)-(51) allow finding steady-state solutions directly. We implemented these equations using standard MATLAB operators, such as matrix inverse and matrix exponential.

We defined the following vectors, each of size N, which represent the mean ages of mitochondria in the stationary, anterograde, and retrograde states in the demand sites, respectively:

$$\mathbf{a}_{s} = \left(\overline{c}_{1}, ..., \overline{c}_{N}\right), \; \mathbf{a}_{a} = \left(\overline{c}_{N+1}, ..., \overline{c}_{2N}\right), \; \mathbf{a}_{r} = \left(\overline{c}_{2N+1}, ..., \overline{c}_{3N}\right). \tag{52}$$

3. Results

3.1. Total length of mitochondria per unit axon length in the demand sites and mitochondria fluxes between the demand sites

Model parameters were chosen using the computational study of Agrawal and Koslover (2021), which found parameter values that optimized mitochondrial health. The parameter values used in our research are summarized in Table S2.

For $\alpha = 0$, $p_s = 0.4$, the distribution of the total length of mitochondria per unit length of the axon is uniform along the length of the axon (Fig. S1a). This is because the model assumes that no mitochondria are destroyed while in the axon, although $(1-\alpha)$ portion of all mitochondria are assumed to be destroyed in the soma when they re-enter the soma from the axon. The uniform distribution displayed in Fig. S1a is consistent with Donovan et al. (2022) who noted that in axons the mitochondrial density is independent of the distance from the soma (Fig. 1C in Donovan et al. 2022). A constant mitochondrial density of 5 mitochondria/100 μm was also reported for growing neuronal processes in *C. elegans* (Mondal et al. 2021).

The return of 30% ($\alpha = 0.3$, $p_s = 0.4$) of exiting mitochondria back to the axon results in the same uniform distribution of mitochondria along the axon length (Fig. S1a). This is because we assumed that the total flux of mitochondria entering the first demand site is the same for all cases computed in this paper. The flux is independent of what portion of returning mitochondria re-enter the axon (Eq. (45)). If more mitochondria re-enter the axon (which corresponds to a greater value of α), the flux of newly synthesized mitochondria entering the first demand site in our model is reduced to keep the total flux of mitochondria entering the first demand site (newly synthesized plus returning, Fig. 2) the same.

The reduction of parameter p_s, which characterizes the rate of mitochondria transition to the stationary state (Fig. 2), to 0.1, resulted in a reduction of the total length of mitochondria per unit length in the stationary state by approximately a factor of 4, which is due to fewer mitochondria transitioning to the stationary state (Fig. S1b). The increase of the value of α to 0.3 did not change the distributions of the total length of mitochondria per unit axonal length (Fig. S1b). This is because, according to our assumptions, the change of α does not affect the flux of mitochondria entering the most proximal demand site.

Anterograde and retrograde fluxes between the compartments are also independent of the values of α and p_s and are uniform along the axon length (Fig. S2a,b).

3.2. Mean age and age density distributions of mitochondria

For $p_s = 0.4$ and $\alpha = 0$ the mean age of mitochondria increases gradually from the most proximal to the most distal demand site. The mean age of anterograde mitochondria is the smallest, the mean age of stationary mitochondria is in the middle, and the mean age of retrograde

mitochondria is the greatest. The mean age of stationary mitochondria in the most distal demand site is approximately 21 h (Fig. 3a).

The mean age for mitochondria for $p_s = 0.4$ and $\alpha = 0$ roughly follows the same trend (an increase from the most proximal to the most distal demand site), but it is now much greater. The mean age of stationary mitochondria in the most distal demand site is now approximately 36 h (Fig. 3b). This is because for $\alpha = 0.3$ the flux of mitochondria entering the axon includes mitochondria that leave the axon moving retrogradely (Fig. 2). We thus successfully simulated the situation described in Mandal et al. (2021) that suggests that older mitochondria appear in the axon due to return of mitochondria leaving the axon, which turn around and return to the axon in the anterograde component. It should be noted that the real situation is even more complicated, since mitochondria returning to the axon are most likely repaired in the soma by fusion with newly synthesized mitochondria. Furthermore, moving mitochondria can fuse with stationary mitochondria residing in the axon and exchange mitochondrial proteins (Errea et al. 2015; Misgeld and Schwarz 2017; Agrawal and Koslover 2021). This process will need to be simulated in future versions of the model.

For a smaller value of p_s ($p_s = 0.1$, $\alpha = 0$, Fig. 3c), the mean age of mitochondria is significantly reduced. The mean age of stationary mitochondria in the most distal demand site is now approximately 10 h. This is because the probability of transitioning between moving states (anterograde or retrograde) and the stationary state (Fig. 2) is now much smaller. It is interesting that although the mean age of anterograde and stationary mitochondria increases from the most proximal to the most distal demand site, the age of retrograde mitochondria now decreases from the most proximal to the most distal demand site (Fig. 3c). This is because the exchange between moving and stationary mitochondria is now much less frequent (due to a smaller value of p_s), and mitochondria mostly remain in the same kinetic state (anterograde, stationary, or retrograde). Retrograde mitochondria age as they return from the most distal demand site (site 10) to the most proximal demand site (site 1), which explains why the age of retrograde mitochondria is the largest in the most proximal demand site.

The increase of α ($p_s = 0.1$, $\alpha = 0.3$, Fig. 3d) results in the increase of the mean age of mitochondria in all demand sites, but the trends stay the same. The mean age of the stationary mitochondria in the most distal demand site is now approximately 20 h. The increase in the mean age is due to the return of 30% of mitochondria exiting the most proximal demand site, which turn around and come back to the axon (Fig. 2).

The age density of mitochondria is important to characterize the ranges of mitochondria ages in different kinetic states (anterograde, stationary, and retrograde) in different demand sites. Fig. 4a compares the age densities of mitochondria computed for the base case ($p_s = 0.4$, $\alpha = 0$, red lines) with age densities of mitochondria computed for the case of $p_s = 0.4$, $\alpha = 0.3$, blue lines. The age densities of anterograde mitochondria are more narrow (Fig. 4a). The distribution of age densities becomes wider for stationary mitochondria (Fig. 4b) and even wider for retrograde mitochondria (Fig. 4c). The increase of α from 0 to 0.3, which is especially visible in Fig. 4c, is due to the return of already aged retrograde mitochondria back to the axon. The presence of older mitochondria is consistent with the results reported in Mandal et al. (2021). The peaks on the curves displaying the age density distributions are shifted toward older mitochondria for more distal demand sites (Fig. 4).

The reduction of the rate of mitochondria transition to the stationary state (characterized by p_s) makes the age density distribution of mitochondria ($p_s = 0.1$, $\alpha = 0$, blue curves, Fig. 5) quite complex. The most noticeable change is the bimodal distribution that is visible in Fig. 5c in the solid blue curve displaying the age density of retrograde mitochondria in the most proximal demand site (site 1). The first peak occurs at approximately 1 h. It is explained by mitochondria that recently entered the axon, but then transitioned to the stationary state, and then to the retrograde state (Fig. 2). The second peak occurs at approximately 11 h. It is explained by older mitochondria that travelled to the axon tip and then returned to the most proximal site.

The increase of the value of α (more mitochondria return to recirculation in the axon) while keeping p_s low (small transition rate to the stationary state) makes the tails in age density distributions longer, which means the presence of older mitochondria in the axon, see Metzler and Sierra (2018) ($p_s = 0.1$, $\alpha = 0.3$, blue curves in Fig. 6c). All age density distributions in Figs. 4-6, and in particular in Fig. 6c, are skewed right. This indicates that although the mean ages of mitochondria are of the order of 20 h (see Fig. 3d, which shows mean ages of mitochondria that correspond to the age density distributions depicted by blue lines in Fig. 6c), there are also much older mitochondria present in the axon, which stay in the axon several times longer than 20 h, probably completing several circulations or staying a long time in the stationary state before returning to the mobile pool.

3.3. Sensitivity of the mean age of mitochondria in demand sites to p_s and α

This investigation was performed by computing local sensitivity coefficients, which are first-order partial derivatives of the observables with respect to model parameters (Beck and Arnold 1977; Zadeh and Montas 2010; Zi 2011; Kuznetsov and Kuznetsov 2019). For example, the sensitivity coefficient of the mean age of resident mitochondria in demand sites to parameter α at steady-state (ss) was calculated as follows:

$$\frac{\partial a_{i,ss}}{\partial \alpha} \approx \left. \frac{a_{i,ss}\left(\alpha + \Delta\alpha\right) - a_{i,ss}\left(\alpha\right)}{\Delta\alpha} \right|_{\text{other parameters kept constant}} \qquad (i=1,\ldots,N), \tag{53}$$

where $\Delta\alpha = 10^{-1}\alpha$ (we tested the accuracy by using various step sizes).

To make sensitivity coefficients independent of the magnitude of the parameter whose sensitivity was tested, we calculated non-dimensional relative sensitivity coefficients (Zadeh and Montas 2010; Kacser et al. 1995), which were defined as (for example):

$$S_{\alpha}^{\bar{a}_{i,ss}} = \frac{\alpha}{a_{i,ss}} \frac{\partial a_{i,ss}}{\partial \alpha} \qquad (i=1,\ldots,N). \tag{54}$$

The dimensionless sensitivity of the mean age of mitochondria to the probability that mobile mitochondria would transition to a stationary state at a demand site, p_s, is positive in all demand sites (Fig. 7a). This is because mitochondria spend more time in the stationary state when the stopping probability is larger.

The dimensionless sensitivity of the mean age of mitochondria to the portion of mitochondria that return to the axon after exiting the axon, α, is also positive in all demand sites (Fig. 7b). This is because older mitochondria, which already circulated in the axon, re-enter the axon when the value of α is larger than zero. The number of older mitochondria in the axon thus increases. This is consistent with the results depicted in Fig. 3 (compare the results in Fig. 3a and Fig. 3b, and also the results in Fig. 3c and Fig. 3d). It is interesting to note that the mean age of stationary mitochondria is approximately 10 times more sensitive to α than to p_s (compare Fig. 7b with Fig. 7a).

4. Discussion, limitations of the model, and future directions

We developed a model that accounts for the return of a portion of mitochondria (characterized by parameter α) back to the axon after mitochondria complete circulation in the axon. We

investigated how the mean age and age density distribution of mitochondria depend on α. We also investigated the dependence of the same quantities on p_s.

Bimodal age density distributions are found for a smaller value of p_s ($p_s = 0.1$). The peak corresponding to older mitochondria on the curve displaying the age density distribution of retrograde mitochondria is explained by mitochondria that traveled to the tip of the axon and then traveled back in the retrograde component. The peak corresponding to younger mitochondria on the curve displaying the age density distribution of retrograde mitochondria is explained by mitochondria that transitioned from the anterograde state to the state occupied by stationary mitochondria and then to the retrograde state.

We found that the mean age of stationary mitochondria is very sensitive to parameter α. It is an order of magnitude less sensitive to parameter p_s.

In future research, a model of fusion/fission of mitochondria should be developed. This is especially important because fusion with newly synthesized mitochondria contributes to the replenishment of older mitochondria with new mitochondrial proteins (Mandal et al. 2021). Mitochondria removal via mitophagy (Twig et al. 2008; Wang and Klionsky 2011) also needs to be incorporated in future models.

Acknowledgment

IAK acknowledges the fellowship support of the Paul and Daisy Soros Fellowship for New Americans and the NIH/National Institute of Mental Health (NIMH) Ruth L. Kirchstein NRSA (F30 MH122076-01). AVK acknowledges the support of the National Science Foundation (award CBET-2042834) and the Alexander von Humboldt Foundation through the Humboldt Research Award.

References

Agrawal A, Koslover EF. 2021. Optimizing mitochondrial maintenance in extended neuronal projections. PLOS Computational Biology. 17:e1009073.

Anderson DH. 1983. Compartmental modeling and tracer kinetics. Berlin: Springer.

Beck JV, Arnold KJ. 1977. Parameter estimation in science and engineering. New York: Wiley.

Cheng X, Huang N, Sheng Z. 2022. Programming axonal mitochondrial maintenance and bioenergetics in neurodegeneration and regeneration. Neuron. 110:1899-1923.

Donovan EJ, Agrawal A, Liberman N, Kalai JI, Chua NJ, Koslover EF, Barnhart EL. 2022. Dendrite architecture determines mitochondrial distribution patterns *in vivo*. bioRxiv. 2022.07.01.497972.

Errea O, Moreno B, Gonzalez-Franquesa A, Garcia-Roves PM, Villoslada P. 2015. The disruption of mitochondrial axonal transport is an early event in neuroinflammation. Journal of Neuroinflammation. 12:152.

Fan T, Xia L, Han Y. 2001. Mitochondrion and apoptosis. Acta Biochimica Et Biophysica Sinica. 33:7-12.

Ferree AW, Trudeau K, Zik E, Benador IY, Twig G, Gottlieb RA, Shirihai OS. 2013. MitoTimer probe reveals the impact of autophagy, fusion, and motility on subcellular distribution of young and old mitochondrial protein and on relative mitochondrial protein age. Autophagy. 9:1887-1896.

Hollenbeck PJ, Saxton WM. 2005. The axonal transport of mitochondria. Journal of Cell Science. 118:5411-5419.

Huang N, Li S, Xie Y, Han Q, Xu X, Sheng Z. 2021. Reprogramming an energetic AKT-PAK5 axis boosts axon energy supply and facilitates neuron survival and regeneration after injury and ischemia. Current Biology. 31:3098-+.

Jacquez JA, Simon CP. 1993. Qualitative theory of compartmental-systems. SIAM Review. 35:43-79.

Jacquez JA. 1985. Compartmental analysis in biology and medicine. 2nd ed. University of Michigan Press, Ann Arbor, MI.

Kacser H, Burns J, Fell D. 1995. The control of flux. Biochemical Society Transactions. 23:341-366.

Karamched BR, Bressloff PC. 2017. Effects of cell geometry on reversible vesicular transport. Journal of Physics A-Mathematical and Theoretical. 50:055601.

Kruppa AJ, Buss F. 2021. Motor proteins at the mitochondria cytoskeleton interface. Journal of Cell Science. 134:jcs226084.

Kuznetsov IA, Kuznetsov AV. 2019. Modelling transport and mean age of dense core vesicles in large axonal arbours. Proceedings of the Royal Society A. 475:20190284.

Kuznetsov IA, Kuznetsov AV. 2020. How old are dense-core vesicles residing in en passant boutons: Simulation of the mean age of dense-core vesicles in axonal arbours accounting for resident and transiting vesicle populations. Proceedings of the Royal Society A-Mathematical Physical and Engineering Sciences. 476:20200454.

Kuznetsov IA, Kuznetsov AV. 2019. Investigating sensitivity coefficients characterizing the response of a model of tau protein transport in an axon to model parameters. Computer Methods in Biomechanics and Biomedical Engineering. 22:71-83.

Kuznetsov IA, Kuznetsov A, V. 2022a. Computation of the mitochondrial age distribution along the axon length. Computer Methods in Biomechanics and Biomedical Engineering. https://doi.org/10.1080/10255842.2022.2128784.

Kuznetsov IA, Kuznetsov A, V. 2022b. Effects of axon branching and asymmetry between the branches on transport, mean age, and age density distributions of mitochondria in neurons: A computational study. International Journal for Numerical Methods in Biomedical Engineering. 38:e3648.

Lees RM, Johnson JD, Ashby MC. 2020. Presynaptic boutons that contain mitochondria are more stable. Frontiers in Synaptic Neuroscience. 11:37.

Lewis TL, Jr., Turi GF, Kwon S, Losonczy A, Polleux F. 2016. Progressive decrease of mitochondrial motility during maturation of cortical axons in vitro and in vivo. Current Biology. 26:2602-2608.

Mandal A, Wong HC, Pinter K, Mosqueda N, Beirl A, Lomash RM, Won S, Kindt KS, Drerup CM. 2021. Retrograde mitochondrial transport is essential for organelle distribution and health in zebrafish neurons. Journal of Neuroscience. 41:1371-1392.

Melkov A, Abdu U. 2018. Regulation of long-distance transport of mitochondria along microtubules. Cellular and Molecular Life Sciences. 75:163-176.

Metzler H, Muller M, Sierra CA. 2018. Transit-time and age distributions for nonlinear time-dependent compartmental systems. Proceedings of the National Academy of Sciences of the United States of America. 115:1150-1155.

Metzler H, Sierra CA. 2018. Linear autonomous compartmental models as continuous-time markov chains: Transit-time and age distributions. Mathematical Geosciences. 50:1-34.

Misgeld T, Schwarz TL. 2017. Mitostasis in neurons: Maintaining mitochondria in an extended cellular architecture. Neuron. 96:651-666.

Mogre SS, Brown A, I., Koslover EF. 2020. Getting around the cell: Physical transport in the intracellular world. Physical Biology. 17:061003.

Mondal S, Dubey J, Awasthi A, Sure GR, Vasudevan A, Koushika SP. 2021. Tracking mitochondrial density and positioning along a growing neuronal process in individual C. elegans neuron using a long-term growth and ImagingMicrofluidic device. Eneuro. 8:0360-20.2021.

Narayanareddy BRJ, Vartiainen S, Hariri N, O'Dowd DK, Gross SP. 2014. A biophysical analysis of mitochondrial movement: Differences between transport in neuronal cell bodies versus processes. Traffic. 15:762-771.

Patel PK, Shirihai O, Huang KC. 2013. Optimal dynamics for quality control in spatially distributed mitochondrial networks. PLOS Computational Biology. 9:e1003108.

Picard M, McEwen BS. 2018. Psychological stress and mitochondria: A systematic review. Psychosomatic Medicine. 80:141-153.

Safiulina D, Kaasik A. 2013. Energetic and dynamic: How mitochondria meet neuronal energy demands. PLOS Biology. 11:e1001755.

Ten V, Galkin A. 2019. Mechanism of mitochondrial complex I damage in brain ischemia/reperfusion injury. A hypothesis. Molecular and Cellular Neuroscience. 100:103408.

Trushina E. 2016. A shape shifting organelle: Unusual mitochondrial phenotype determined with three-dimensional electron microscopy reconstruction. Neural Regeneration Research. 11:900-901.

Twig G, Elorza A, Molina AJA, Mohamed H, Wikstrom JD, Walzer G, Stiles L, Haigh SE, Katz S, Las G, Alroy J, Wu M, Py BF, Yuan J, Deeney JT, Corkey BE, Shirihai OS. 2008. Fission and selective fusion govern mitochondrial segregation and elimination by autophagy. EMBO Journal. 27:433-446.

Wang K, Klionsky DJ. 2011. Mitochondria removal by autophagy. Autophagy. 7:297-300.

Zadeh KS, Montas HJ. 2010. A class of exact solutions for biomacromolecule diffusion-reaction in live cells. Journal of Theoretical Biology. 264:914-933.

Zi Z. 2011. Sensitivity analysis approaches applied to systems biology models. IET Systems Biology. 5:336-346.

Figure captions

Fig. 1. (a) Schematic diagram of a neuron with an axon that is assumed to contain *N* energy demand sites. Demand sites are numbered starting with the most proximal (site 1) to the most distal (site *N*). *Figure generated with the aid of servier medical art, licensed under a creative commons attribution 3.0 generic license. http://Smart.servier.com.*

*Fig. 2. A d*iagram of a compartmental model showing transport in the compartments surrounding the demand sites in the axon. Arrows show mitochondria exchange between the transiting (anterograde and retrograde) states in adjacent demand sites, mitochondria capture into the stationary state and re-release from the stationary state. A portion of mitochondria re-enter the axon, and the rest return to the soma for degradation. Newly synthesized mitochondria entering the axon from the soma are assumed to have zero age.

Fig. 3. Mean age of stationary, anterogradely moving, and retrogradely moving mitochondria. (a) $p_s = 0.4$, $\alpha = 0$; (b) $p_s = 0.4$, $\alpha = 0.3$; (c) $p_s = 0.1$, $\alpha = 0$; (d) $p_s = 0.1$, $\alpha = 0.3$.

Fig. 4. (a) Age density of anterogradely moving mitochondria in various demand sites. (b) Age density of mitochondria in the stationary state in various demand sites. (c) Age density of retrogradely moving mitochondria in various demand sites. Two sets of parameter values: $p_s = 0.4$, $\alpha = 0$ (base case) and $p_s = 0.4$, $\alpha = 0.3$.

Fig. 5. (a) Age density of anterogradely moving mitochondria in various demand sites. (b) Age density of mitochondria in the stationary state in various demand sites. (c) Age density of retrogradely moving mitochondria in various demand sites. Two sets of parameter values: $p_s = 0.4$, $\alpha = 0$ (base case) and $p_s = 0.1$, $\alpha = 0$.

Fig. 6. (a) Age density of anterogradely moving mitochondria in various demand sites. (b) Age density of mitochondria in the stationary state in various demand sites. (c) Age density of retrogradely moving mitochondria in various demand sites. Two sets of parameter values: $p_s = 0.4$, $\alpha = 0$ (base case) and $p_s = 0.1$, $\alpha = 0.3$.

Fig. 7. (a) Dimensionless sensitivity of the mean age of mitochondria to the probability that mobile mitochondria would transition to a stationary state at a demand site, p_s, versus the site number. Computations were performed with $\Delta p_s = 10^{-1} p_s$. A close result was obtained for $\Delta p_s = 10^{-2} p_s$. (b) Dimensionless sensitivity of the mean age of mitochondria to the portion of mitochondria that return to the axon after exiting the axon, α, versus the site number.

Computations were performed with $\Delta\alpha = 10^{-1}\alpha$. A close result was obtained for $\Delta\alpha = 10^{-2}\alpha$. Sensitivities are analyzed around $p_s = 0.1$ s^{-1}, $\alpha = 0.3$.

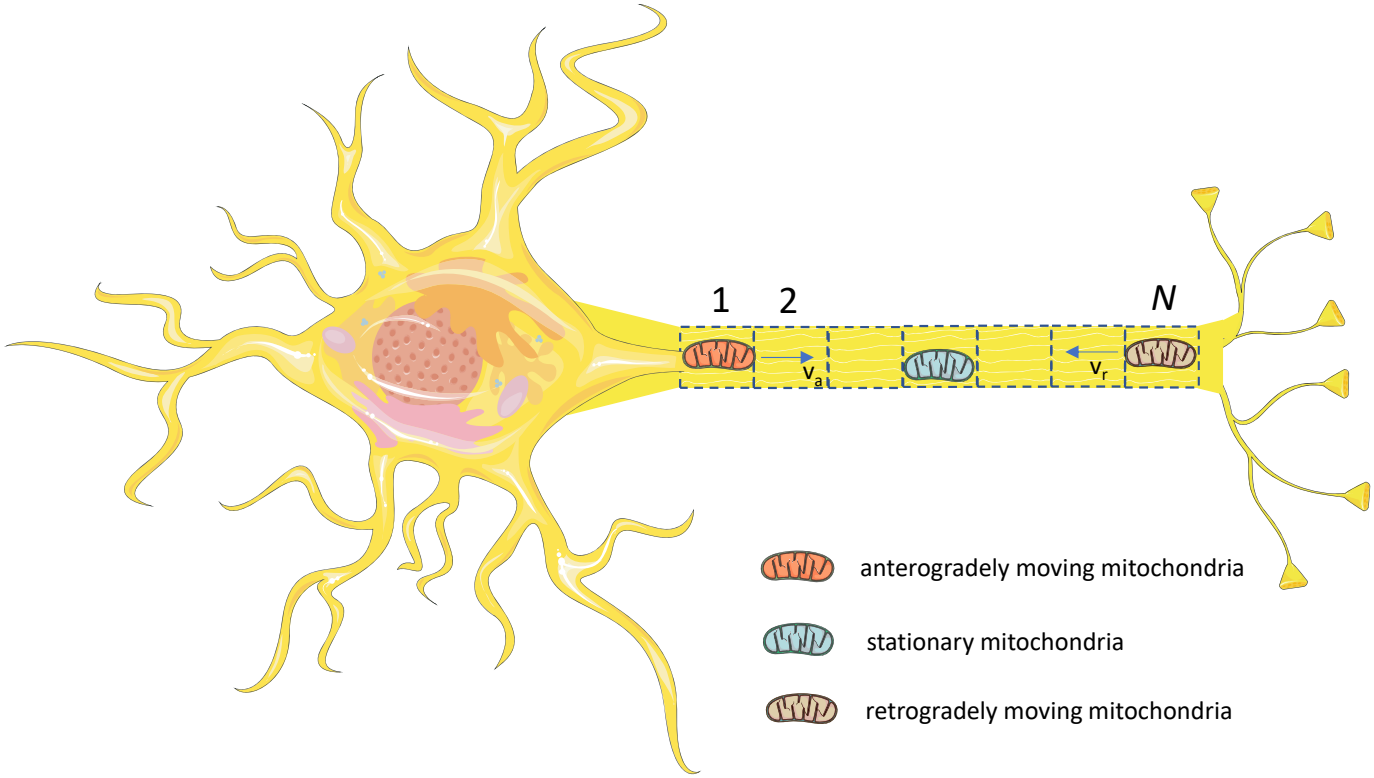
1
2
N
v_a
v_r
anterogradely moving mitochondria
stationary mitochondria
retrogradely moving mitochondria

Figure 1

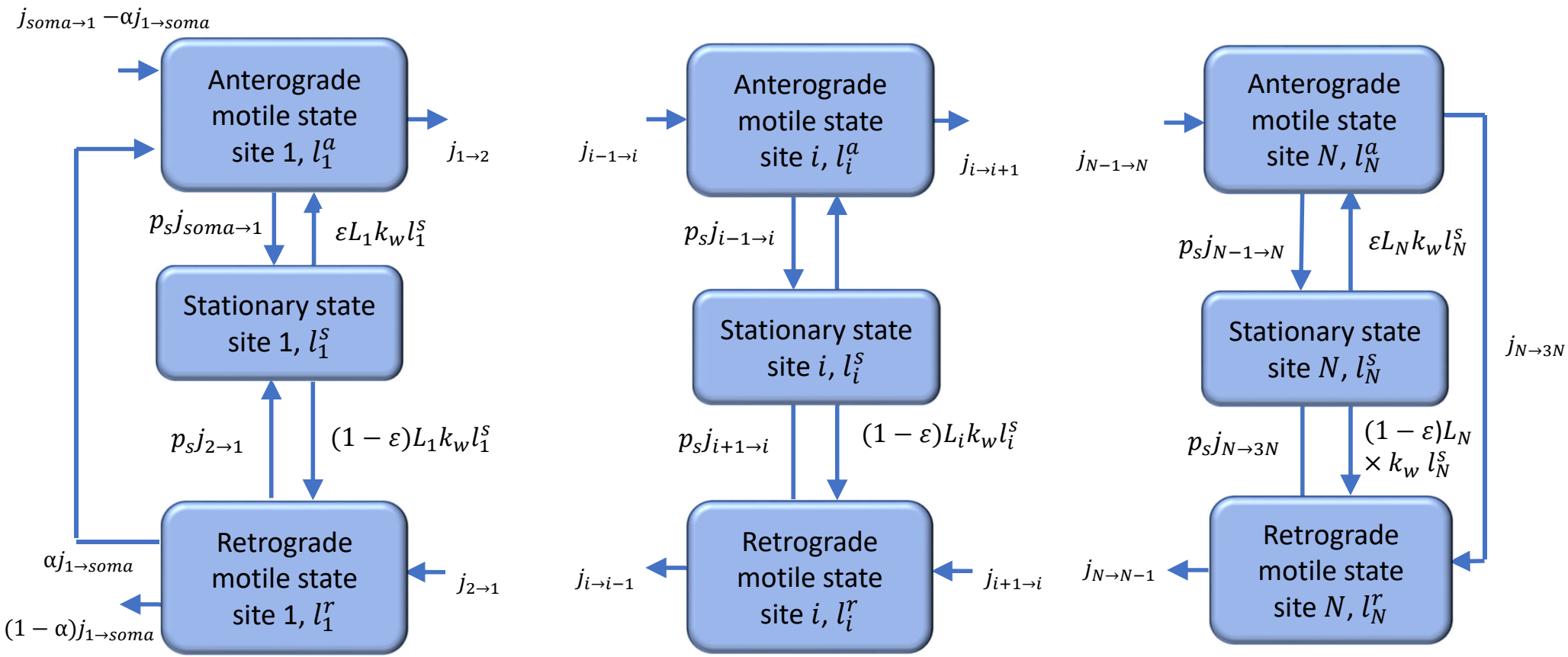
$j_{soma\to1} - \alpha j_{1\to soma}$
Anterograde motile state site 1, l_1^a
$j_{1\to2}$
$p_s j_{soma\to1}$
$\varepsilon L_1 k_w l_1^s$
Stationary state site 1, l_1^s
$p_s j_{2\to1}$
$(1-\varepsilon) L_1 k_w l_1^s$
$\alpha j_{1\to soma}$
Retrograde motile state site 1, l_1^r
$j_{2\to1}$
$(1-\alpha) j_{1\to soma}$
$j_{i-1\to i}$
Anterograde motile state site i, l_i^a
$j_{i\to i+1}$
$p_s j_{i-1\to i}$
Stationary state site i, l_i^s
$p_s j_{i+1\to i}$
$(1-\varepsilon) L_i k_w l_i^s$
$j_{i\to i-1}$
Retrograde motile state site i, l_i^r
$j_{i+1\to i}$
$j_{N-1\to N}$
Anterograde motile state site N, l_N^a
$p_s j_{N-1\to N}$
$\varepsilon L_N k_w l_N^s$
Stationary state site N, l_N^s
$j_{N\to3N}$
$p_s j_{N\to3N}$
$(1-\varepsilon) L_N \times k_w\ l_N^s$
$j_{N\to N-1}$
Retrograde motile state site N, l_N^r

Figure 2

(a)

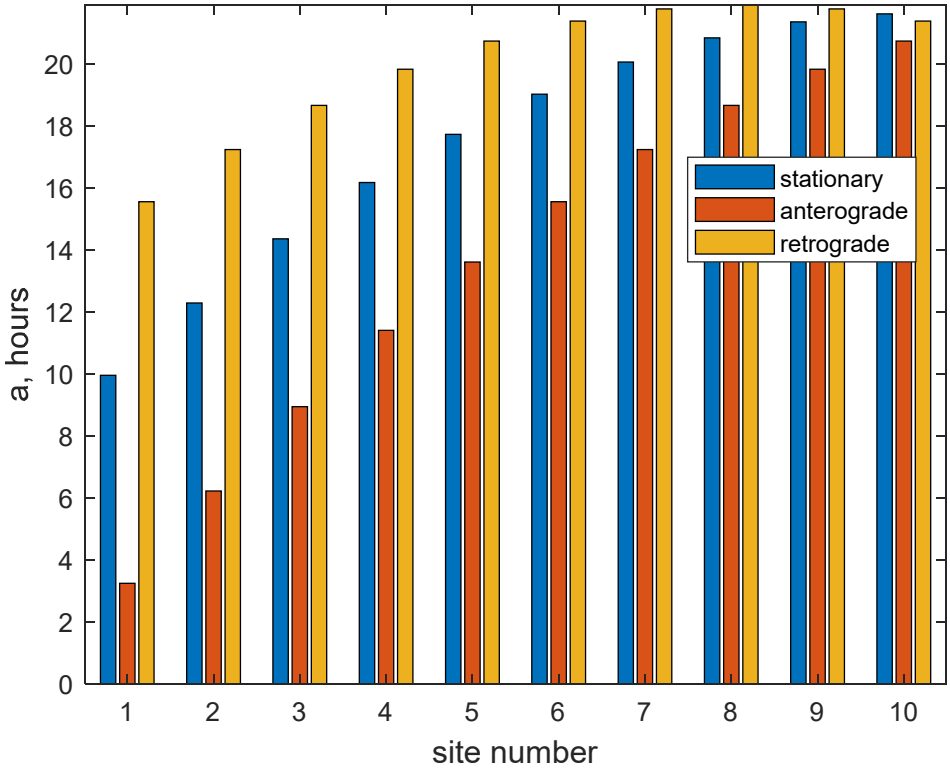

(b)

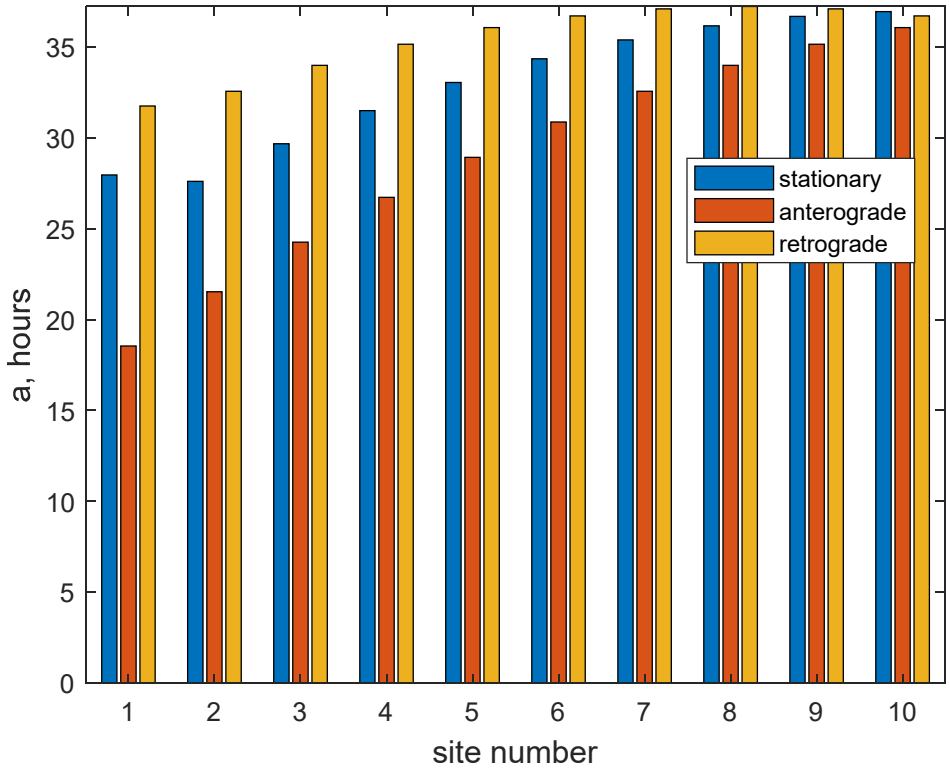

Figure 3a,b

(a)

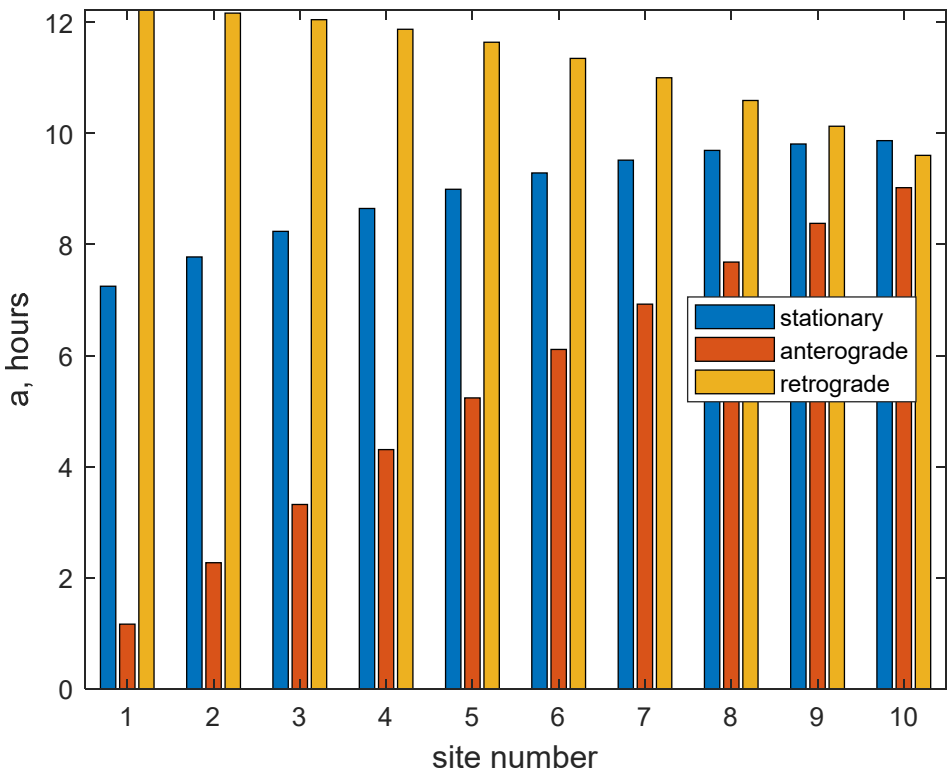

(b)

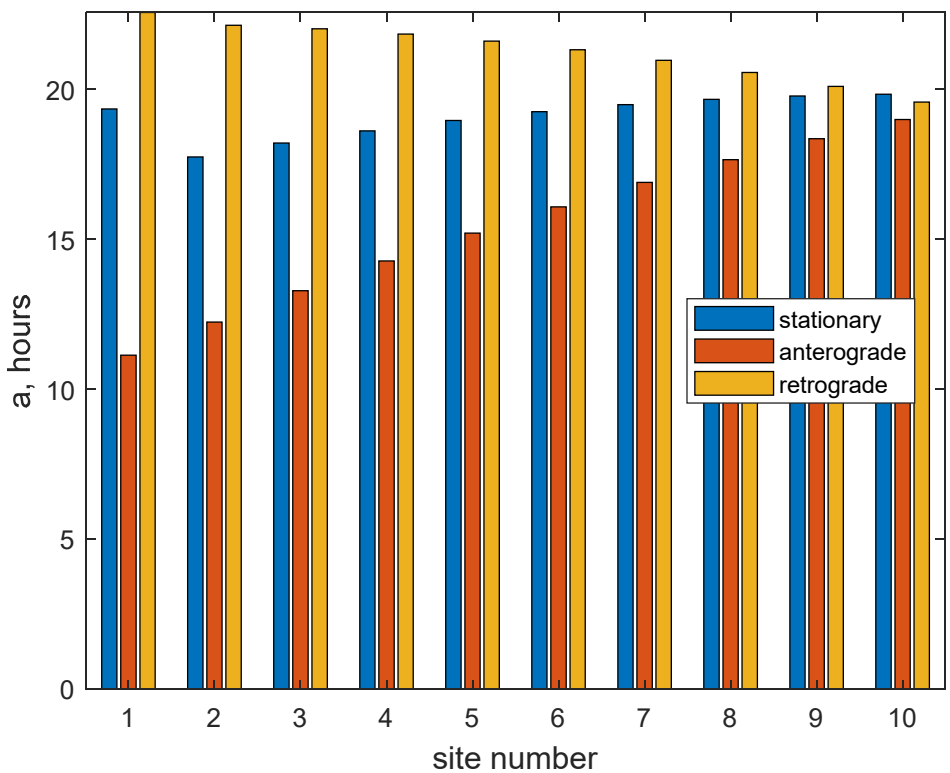

Figure 3c,d

(a)

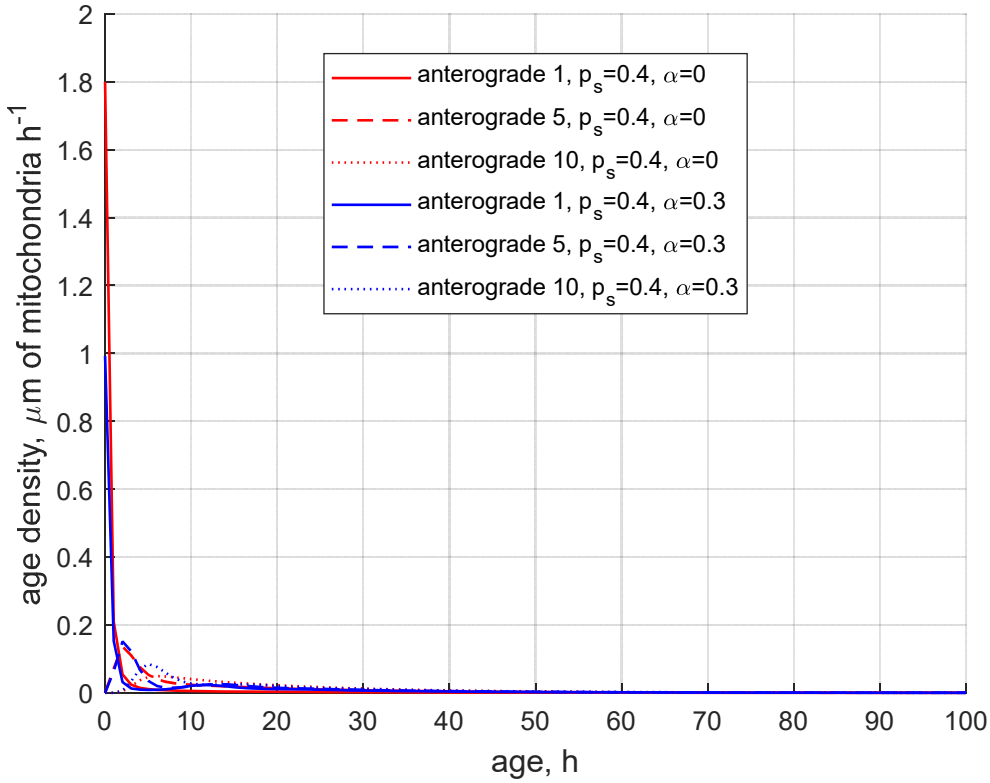

(b)

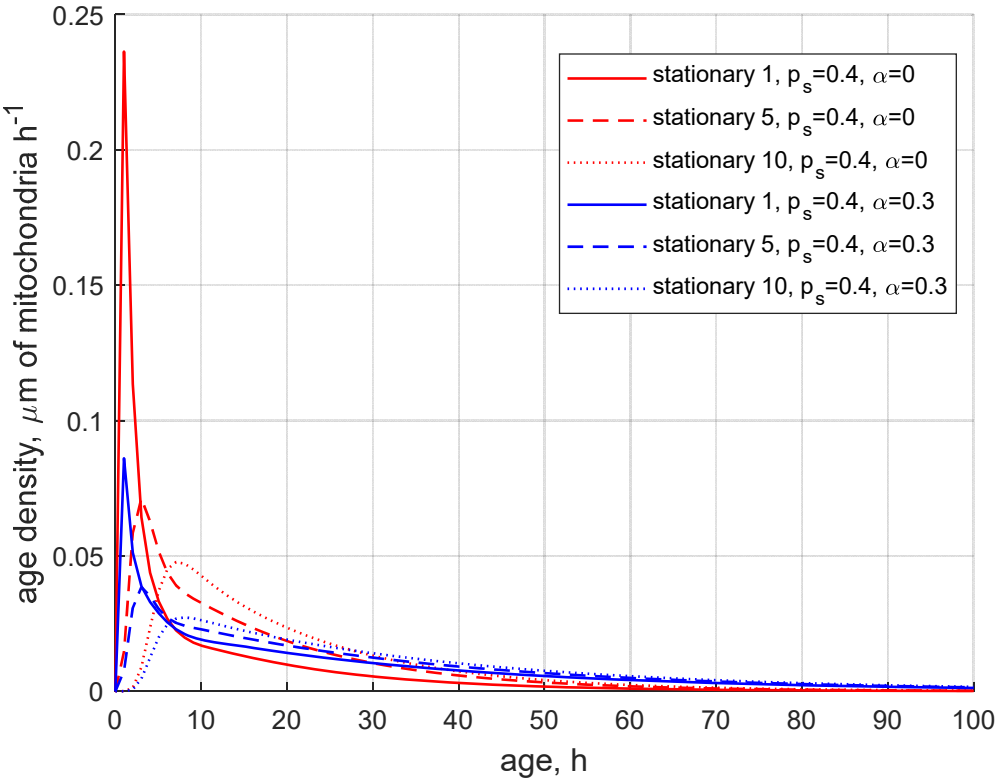

Figure 4a,b

(c)

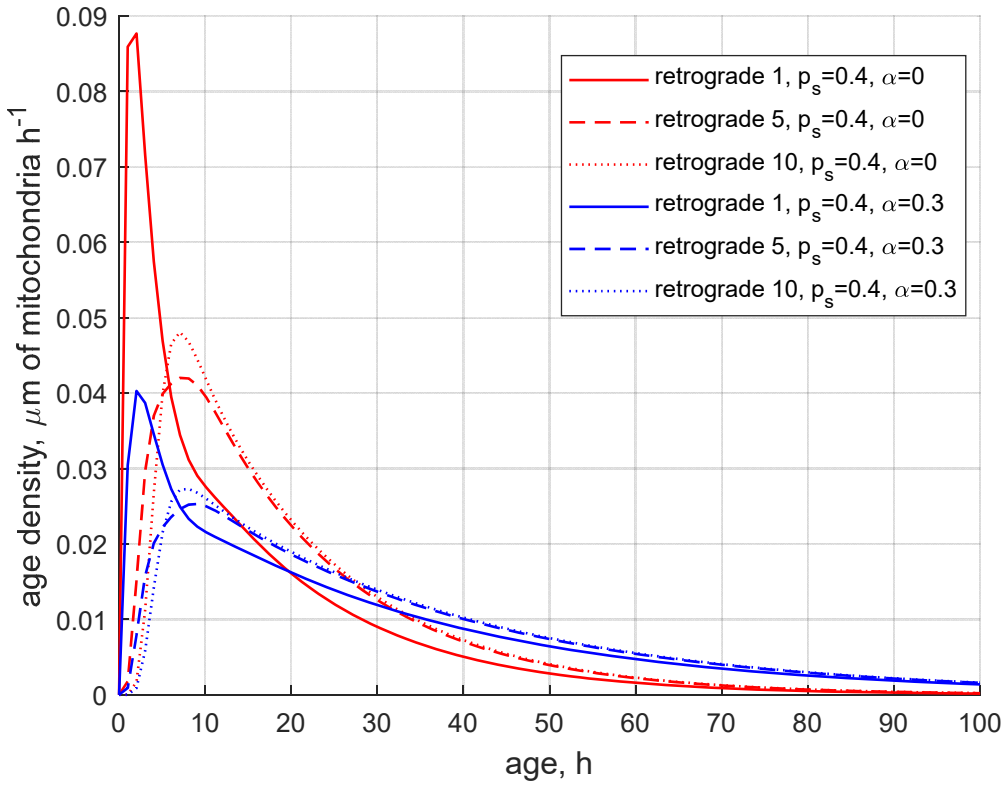
0.09
0.08
0.07
0.06
0.05
0.04
0.03
0.02
0.01
0
age density, μm of mitochondria h^{-1}
0
10
20
30
40
50
60
70
80
90
100
age, h
retrograde 1, p_s=0.4, α=0
retrograde 5, p_s=0.4, α=0
retrograde 10, p_s=0.4, α=0
retrograde 1, p_s=0.4, α=0.3
retrograde 5, p_s=0.4, α=0.3
retrograde 10, p_s=0.4, α=0.3

Figure 4c

(a)

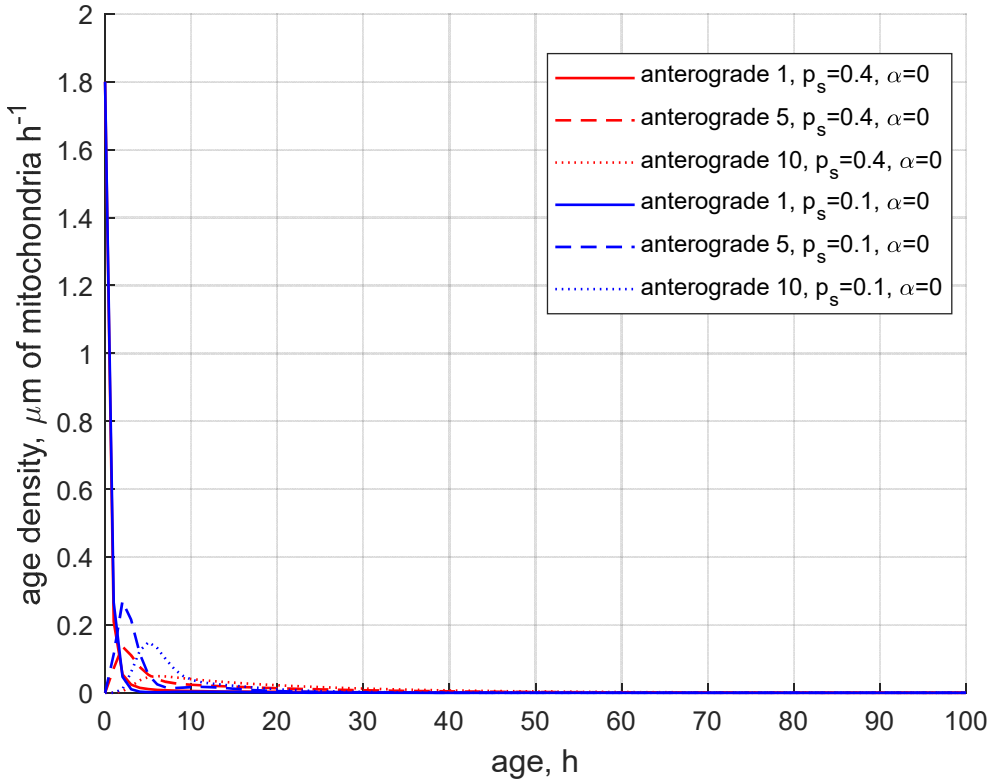

(b)

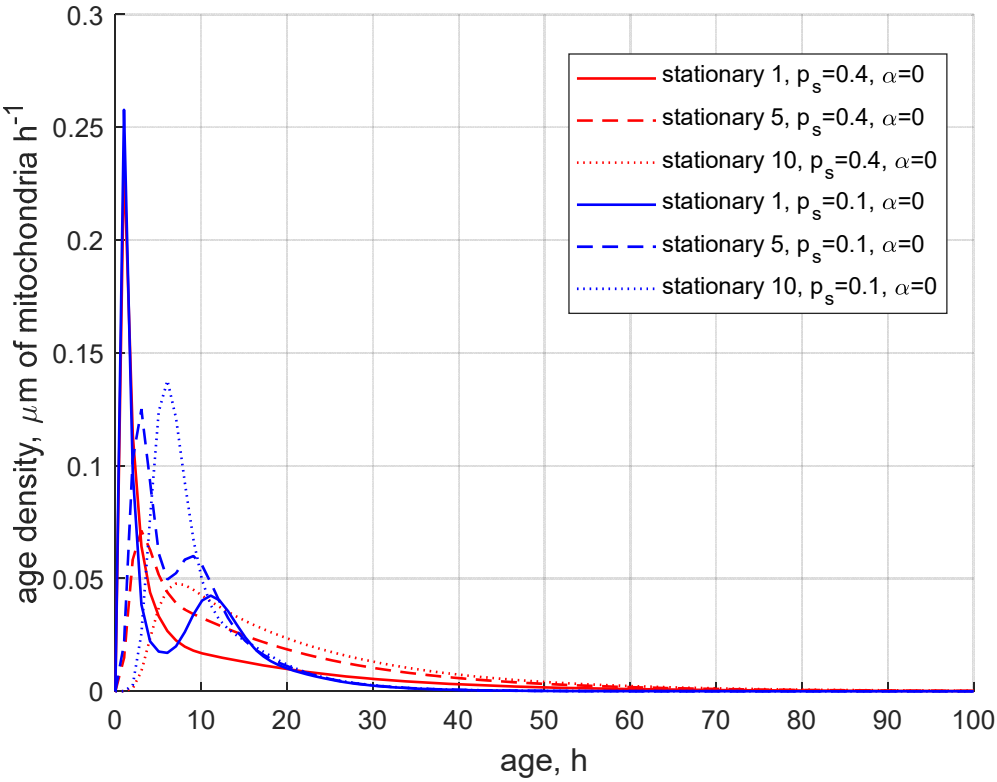

Figure 5a,b

(c)

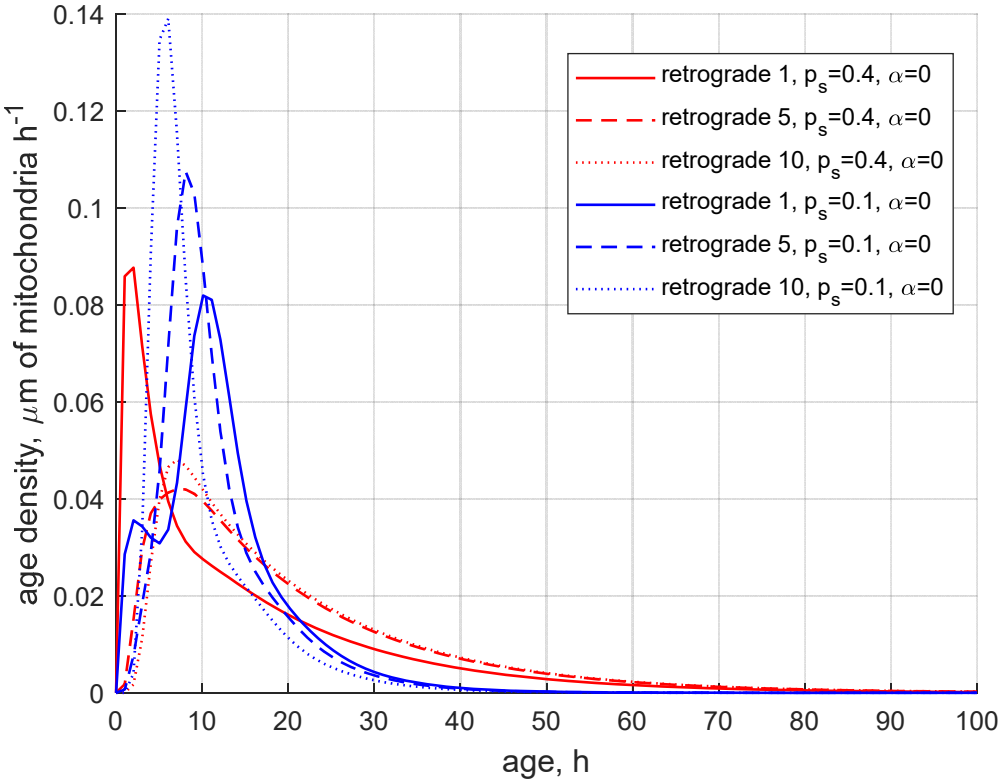
0.14
0.12
0.1
0.08
0.06
0.04
0.02
0
age density, μm of mitochondria h^{-1}
0
10
20
30
40
50
60
70
80
90
100
age, h
retrograde 1, p_s=0.4, α=0
retrograde 5, p_s=0.4, α=0
retrograde 10, p_s=0.4, α=0
retrograde 1, p_s=0.1, α=0
retrograde 5, p_s=0.1, α=0
retrograde 10, p_s=0.1, α=0

Figure 5c

(a)

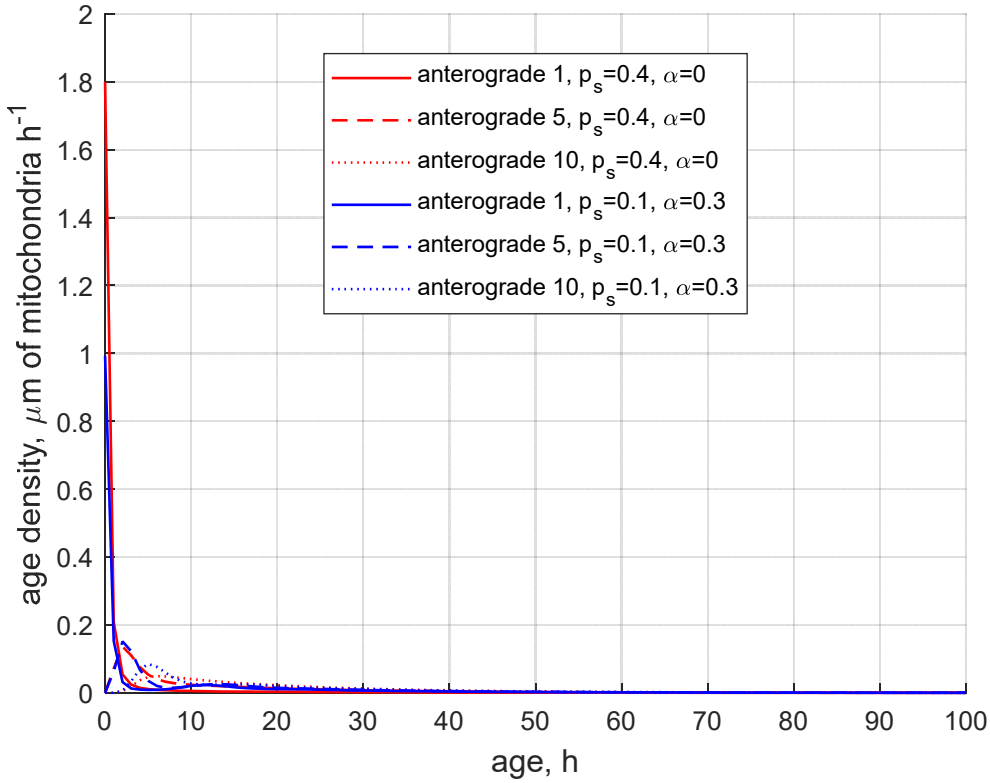

(b)

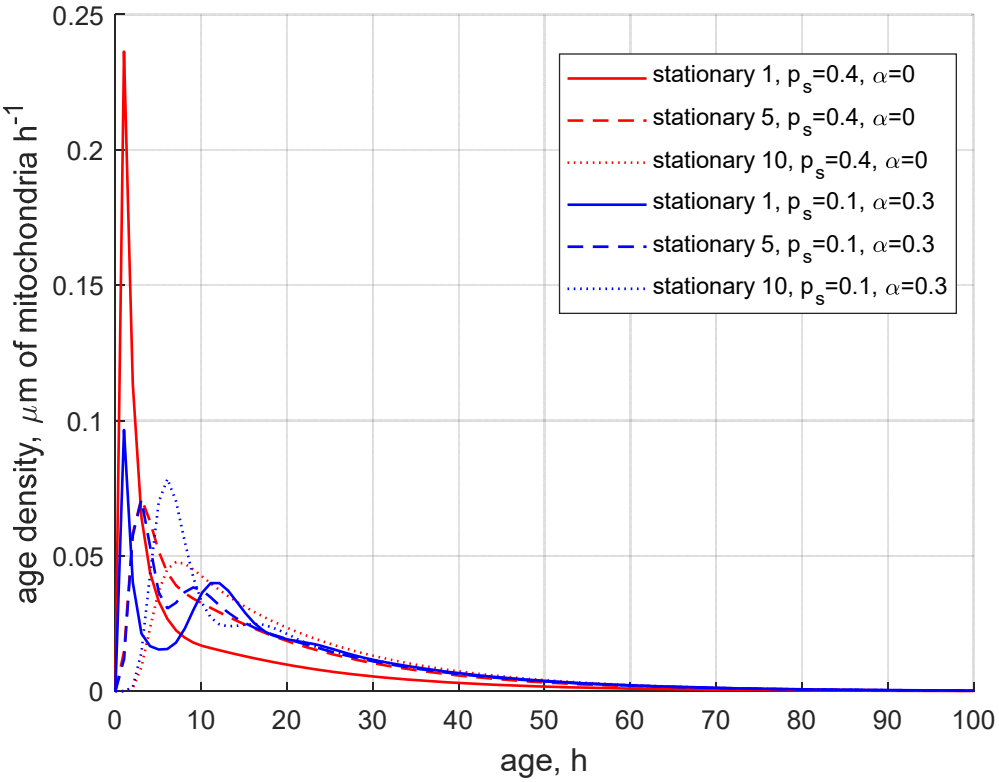

Figure 6a,b

(c)

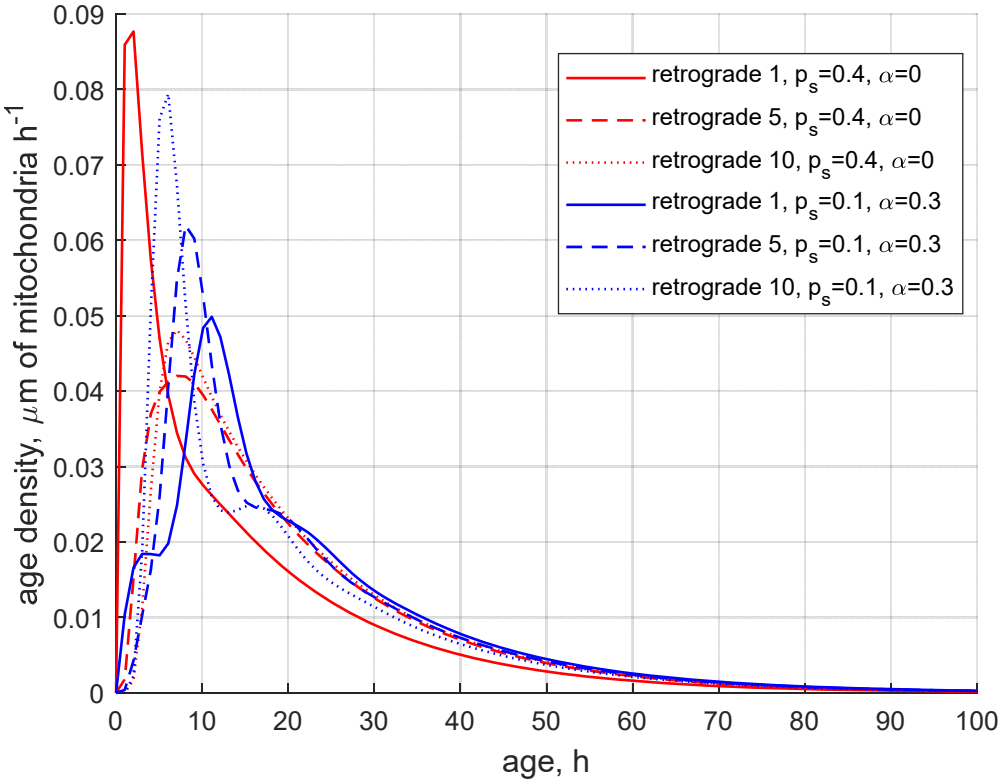
0.09
0.08
0.07
0.06
0.05
0.04
0.03
0.02
0.01
0
age density, μm of mitochondria h-1
0
10
20
30
40
50
60
70
80
90
100
age, h
retrograde 1, ps=0.4, α=0
retrograde 5, ps=0.4, α=0
retrograde 10, ps=0.4, α=0
retrograde 1, ps=0.1, α=0.3
retrograde 5, ps=0.1, α=0.3
retrograde 10, ps=0.1, α=0.3

Figure 6c

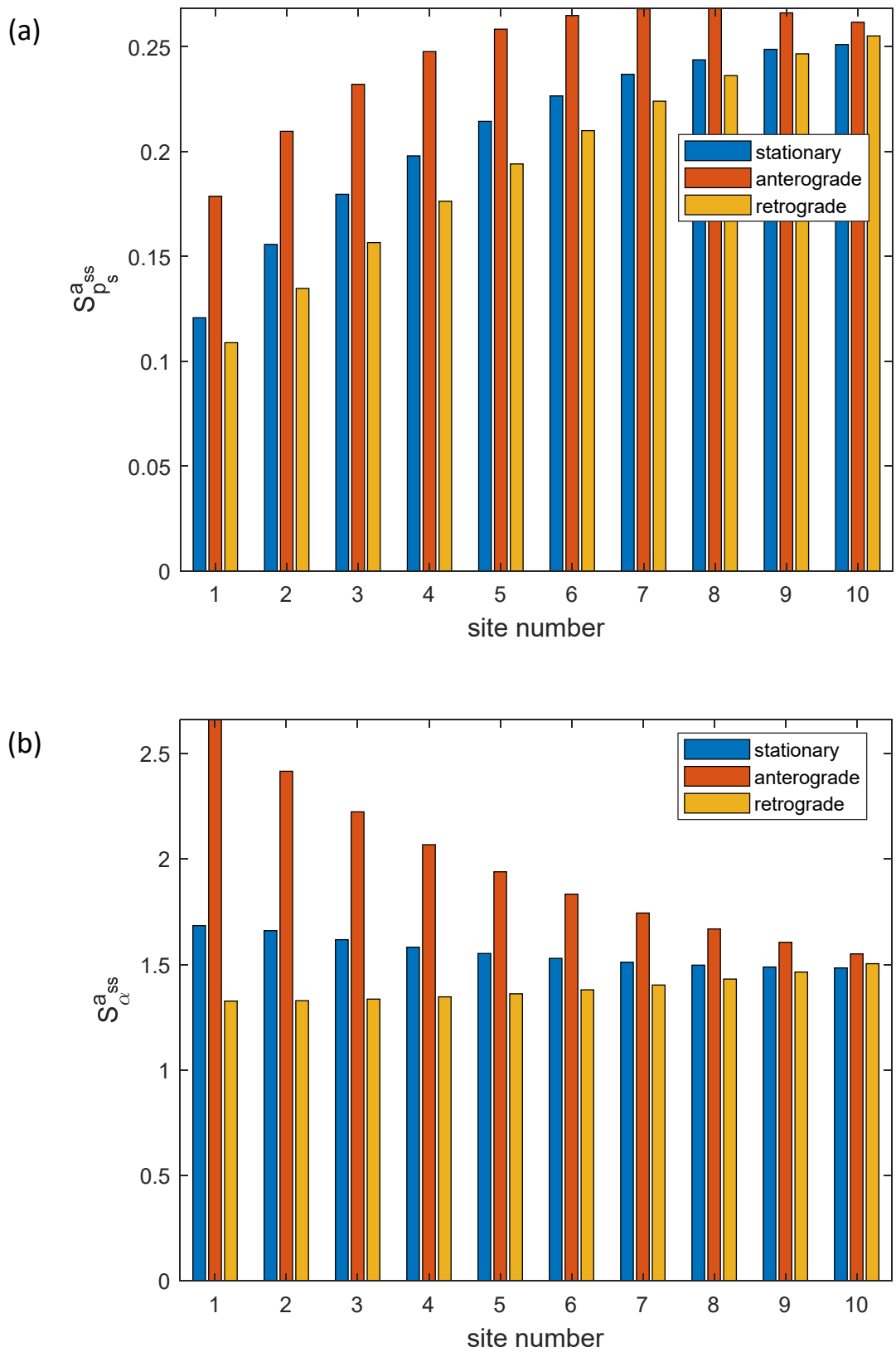
(a)
0.25
0.2
0.15
0.1
0.05
0
$S^{a}_{p^{ss}_{s}}$
stationary
anterograde
retrograde
1
2
3
4
5
6
7
8
9
10
site number
(b)
2.5
2
1.5
1
0.5
0
$S^{a}_{\alpha^{ss}}$
stationary
anterograde
retrograde
1
2
3
4
5
6
7
8
9
10
site number

Figure 7a,b

Effect of mitochondrial circulation on mitochondrial age density distribution

Ivan A. Kuznetsov[(a), (b)] and Andrey V. Kuznetsov[(c)]

[(a)]Perelman School of Medicine, University of Pennsylvania, Philadelphia, PA 19104, USA

[(b)]Department of Bioengineering, University of Pennsylvania, Philadelphia, PA 19104, USA

[(c)]Dept. of Mechanical and Aerospace Engineering, North Carolina State University, Raleigh, NC 27695-7910, USA; e-mail: avkuznet@ncsu.edu

Supplemental Materials

S1. Alternative form of governing equations

An alternative way of stating the conservation equations for the total length of mitochondria in the axon, developed in Kuznetsov and Kuznetsov (2022a), is as follows. The solution of these alternative governing equations is identical to the solution of vector Eq. (1).

Stating the conservation of the total length of stationary mitochondria in the most proximal demand site (site 1, Fig. 2) gives the following equation:

$$L_1 \frac{dl_1^s}{dt} = p_s \left(j_{soma\to 1} + j_{2\to 1} \right) - L_1 k_w l_1^s \,. \tag{S1}$$

Stating the conservation of the total length of anterograde mitochondria in demand site 1 gives the following equation (Fig. 2):

$$L_1 \frac{dl_1^a}{dt} = j_{soma\to 1} - p_s j_{soma\to 1} - j_{1\to 2} + \varepsilon L_1 k_w l_1^s \,. \tag{S2}$$

Stating the conservation of the total length of retrograde mitochondria in demand site 1 results in the following equation (Fig. 2):

$$L_1 \frac{dl_1^r}{dt} = j_{2\to 1} - p_s j_{2\to 1} - j_{1\to soma} + \left(1-\varepsilon\right) L_1 k_w l_1^s \,. \tag{S3}$$

Stating the conservation of the total length of stationary mitochondria in the ith demand site (i=2,...,N-1) leads to the following equation (Fig. 2):

$$L_i \frac{dl_i^s}{dt} = p_s \left(j_{i-1\to i} + j_{i+1\to i} \right) - L_i k_w l_i^s \,. \tag{S4}$$

Stating the conservation of the total length of anterograde mitochondria in the *i*th demand site (*i*=2,...,*N*-1) leads to the following equation (Fig. 2):

$$L_i \frac{dl_i^a}{dt} = j_{i-1\to i} - p_s j_{i-1\to i} - j_{i\to i+1} + \varepsilon L_i k_w l_i^s . \tag{S5}$$

Stating the conservation of the total length of retrograde mitochondria in the *i*th demand site (*i*=2,...,*N*-1) results in the following equation (Fig. 2):

$$L_i \frac{dl_i^r}{dt} = j_{i+1\to i} - p_s j_{i+1\to i} - j_{i\to i-1} + \left(1-\varepsilon\right) L_i k_w l_i^s . \tag{S6}$$

As suggested by Agrawal and Koslover (2021), mitochondria that reach the distal end of the axon instantaneously switch from anterograde motors (kinesins) to retrograde motors (dyneins) and continue moving retrogradely in the axon. This is simulated by $j_{N\to 3N}$ flux (Fig. 2). Stating the conservation of the total length of stationary mitochondria in the most distal demand site (site *N*) leads to the following equation (Fig. 2):

$$L_N \frac{dl_N^s}{dt} = p_s \left(j_{N-1\to N} + j_{N\to 3N} \right) - L_N k_w l_N^s . \tag{S7}$$

Stating the conservation of the total length of anterograde mitochondria in the most distal demand site (site *N*) leads to the following equation (Fig. 2):

$$L_N \frac{dl_N^a}{dt} = j_{N-1\to N} - p_s j_{N-1\to N} - j_{N\to N-1} + \varepsilon L_N k_w l_N^s . \tag{S8}$$

Stating the conservation of the total length of retrograde mitochondria in the most distal demand site (site *N*) leads to the following equation (Fig. 2):

$$L_N \frac{dl_N^r}{dt} = j_{N\to 3N} - p_s j_{N\to 3N} - j_{N\to N-1} + \left(1-\varepsilon\right) L_N k_w l_N^s . \tag{S9}$$

To obtain steady-state solutions, we set the left-hand side of Eqs. (S1)-(S9) to zero and solved the obtained system of linear equations for the total length of mitochondria per unit length of the axon in each compartment. Steady-state solutions of Eqs. (S1)-(S9) coincide with those displayed in Fig. S1, which validates our implementation of matrix B given by Eqs. (4)-(34) and Eq. (47).

S2. Supplementary tables

Table S1. Dependent variables in the model of mitochondrial transport and accumulation in the axon.

Symbol	Definition	Units
l_i^s	Total length of stationary mitochondria per unit length of the axon in the compartment by the *i*th demand site	(μm of mitochondria)/μm
l_i^a	Total length of anterogradely moving mitochondria per unit length of the axon in the compartment by the *i*th demand site	(μm of mitochondria)/μm
l_i^r	Total length of retrogradely moving mitochondria per unit length of the axon in the compartment by the *i*th demand site	(μm of mitochondria)/μm
$j_{a\to b}$	Flux of mitochondria length from state (compartment) *a* to state (compartment) *b*	(μm of mitochondria) s^{-1}

Table S2. Parameters characterizing mitochondrial transport and accumulation in the axon.

Symbol	Definition	Units	Value or range	Reference(s)	Value used in computations
v_a	Average velocity of anterogradely moving mitochondria	$\mu m\, s^{-1}$	0.5	Agrawal and Koslover (2021)	0.5
v_r	Average velocity of retrogradely moving mitochondria	$\mu m\, s^{-1}$	0.5	Agrawal and Koslover (2021)	0.5
$j_{soma\to 1}$	Total flux of the length of anterograde mitochondria entering the most proximal demand site. It consists of mitochondria newly synthesized in the soma and mitochondria that just left the axon and re-enter the axon anterogradely	mitochondria s^{-1}	0.0375	Agrawal and Koslover (2021)	0.0375 [a]
L_{ax}	Length of the axon	μm	10^4 - 10^5	Agrawal and Koslover (2021)	10^4
k_w	Kinetic constant characterizing the rate of mitochondria reentry into	s^{-1}	$2\times10^{-4} - 2\times10^{-3}$ [b]	Agrawal and Koslover (2021)	5×10^{-4} [c]

	mobile states (anterograde and retrograde)				
α	Portion of mitochondria that return to the axon after exiting the axon		0-1		0, 0.3
ε	Portion of mitochondria leaving the stationary state that join the anterograde pool; $(1-\varepsilon)$ join the retrograde pool		0.5	Agrawal and Koslover (2021)	0.5
f_s	Fraction of stationary mitochondria		0.5-0.6	Agrawal and Koslover (2021)	0.5
p_s	Probability that mobile mitochondria would transition to a stationary state at a demand site		0.4-0.5 [d]	Agrawal and Koslover (2021)	0.1, 0.4
N	Number of demand sites in the axon		5-100 [e]	Agrawal and Koslover (2021)	10

[a] $j_{soma\to 1}$ was estimated using the formula suggested in Agrawal and Koslover (2021), $Mv/(2L_{ax})$, where M is the number of mitochondria in the axon and v is the average velocity of mitochondria motion in the axon. We used 1,500 mitochondria for M, 0.5 μm/s for v, and 1 cm for L_{ax}.

[b] We used Eq. (4) from Agrawal and Koslover (2021), $f_s = \dfrac{Nvp_s}{L_{ax}k_w + Nvp_s}$. By solving this equation for k_w using values given in Table S2 (for N we used the range 10-100), we obtained that k_w is in the range 2×10^{-4} to 2×10^{-3} s^{-1}.

[c] Kuznetsov and Kuznetsov (2022a) reported that $k_w = 5\times10^{-4}$ s^{-1} leads to the predicted mean age of mitochondria of approximately 21.6 hours, which is consistent with the value that follows from Ferree et al. (2013).

[d] We used $p_s = \dfrac{N_s}{2N}$, where N_s is an average number of stops that a mitochondrion makes during a back and forth journey in the axon (Agrawal and Koslover 2021).

[e] Number of demand sites in a real axon can be much larger than 10.

S3. Supplementary figures

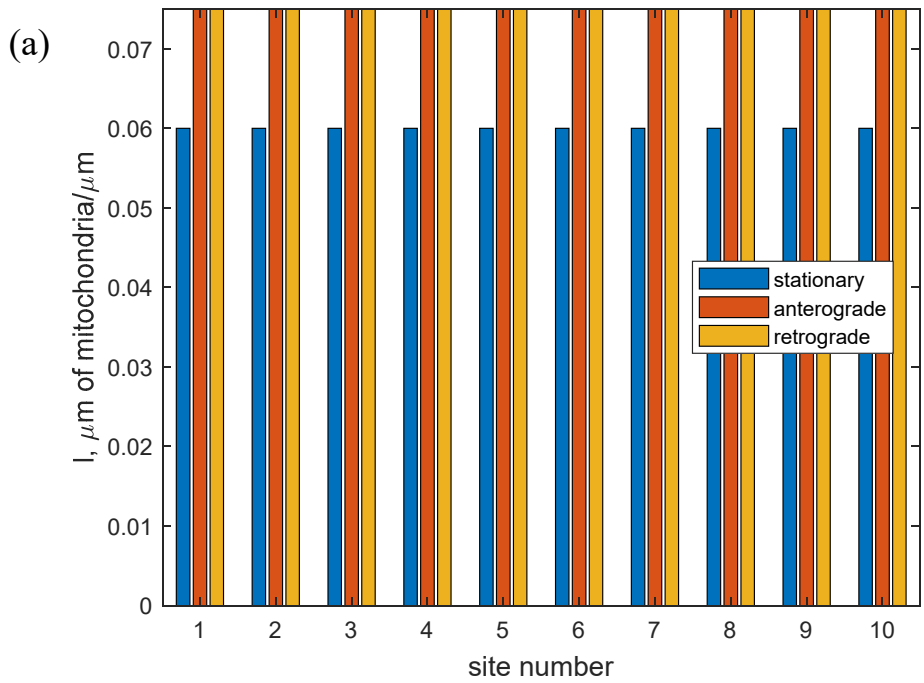

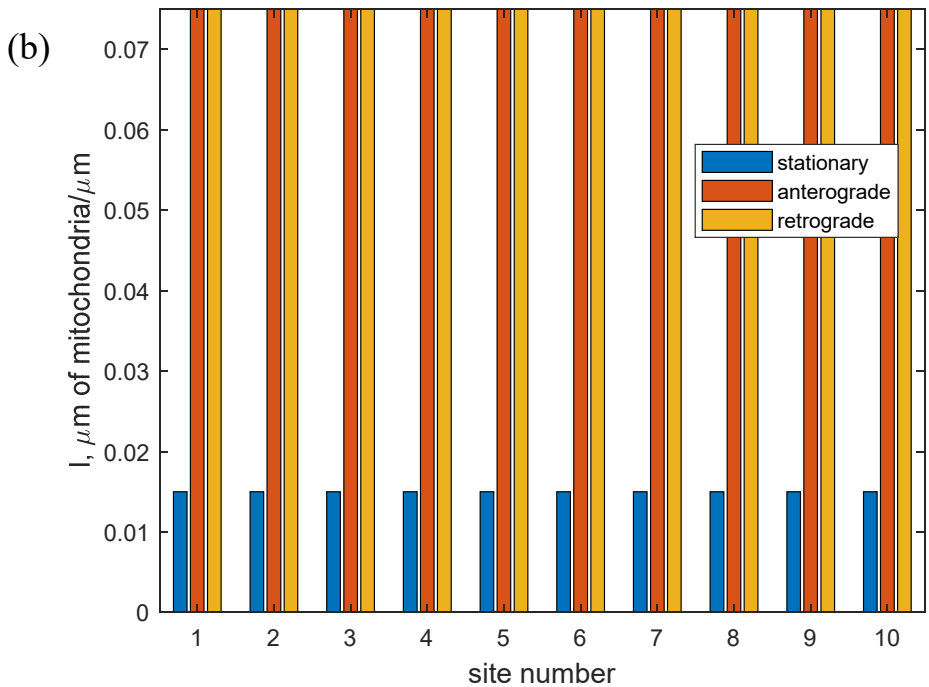

Fig. S1. Steady-state values of the total length of stationary, anterogradely moving, and retrogradely moving mitochondria per unit length of the axon in the compartment by the *i*th demand site. (a) $p_s = 0.4$, the results are independent of the value of α; (b) $p_s = 0.1$, the results are independent of the value of α.

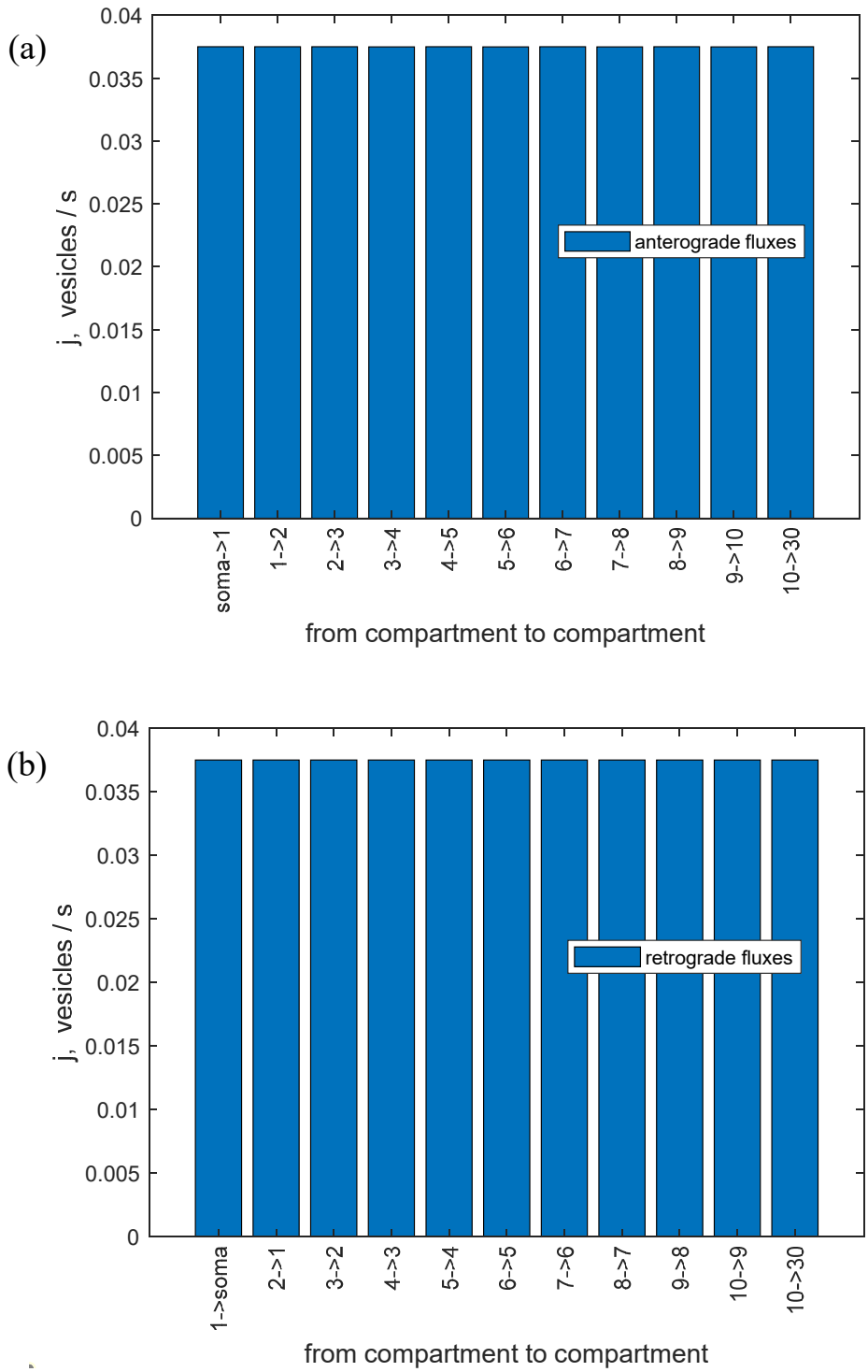

Fig. S2. (a) Anterograde and (b) retrograde fluxes of mitochondria traveling between the compartments. The results are independent of the values of p_s and α.